Polyhedron 29 (2010) 1337–1343

Contents lists available at ScienceDirect

Polyhedron

journal homepage: www.elsevier.com/locate/poly

Synthesis, structure, redox property and ligand replacement reaction of ruthenium(II) complexes containing a terpyridyl ligand with a redox active moiety

Dai Oyama [a,*], Masato Kido [b], Ai Orita [c], Tsugiko Takase [a]

[a] Cluster of Science and Technology, Fukushima University, 1 Kanayagawa, Fukushima 960-1296, Japan
[b] Graduate School of Science and Technology, Fukushima University, 1 Kanayagawa, Fukushima 960-1296, Japan
[c] Faculty of Education, Fukushima University, 1 Kanayagawa, Fukushima 960-1296, Japan

ARTICLE INFO

Article history:
Received 4 November 2009
Accepted 15 December 2009
Available online 23 December 2009

Keywords:
Ruthenium complex
Terpyridine
Crystal structure
Redox property
Ligand replacement reaction

ABSTRACT

Ruthenium(II) complexes bearing a redox-active tridentate ligand 4′-(2,5-dimethoxyphenyl)-2,2′:6′,2″-terpyridine (tpyOMe), analogous to terpyridine, and 2,2′-bipyridine (bpy) were synthesized by the sequential replacement of Cl by CH_3CN and CO on the complex. The new ruthenium complexes were characterized by various methods including IR and NMR. The molecular structures of $[Ru(tpyOMe)(bpy)(CH_3CN)]^{2+}$ and two kinds of $[Ru(tpyOMe)(bpy)(CO)]^{2+}$ were determined by X-ray crystallography. The incorporation of monodentate ligands (Cl, CH_3CN and CO) regulated the energy levels of the MLCT transitions and the metal-centered redox potentials of the complexes. The kinetic data observed in this study indicates that the ligand replacement reaction of $[Ru(tpyOMe)(bpy)Cl]^+$ to $[Ru(tpyOMe)(bpy)(CH_3CN)]^{2+}$ proceeds by a solvent-assisted dissociation process.

1. Introduction

Ruthenium(II) complexes containing polypyridyl ligands such as 2,2′-bipyridine (bpy) and 2,2′:6′,2″-terpyridine (tpy) have been extensively studied as photo- and electrocatalysts due to their accessible redox states [1,2]. Recently, we have reported several ruthenium(II) complexes bearing redox active azopyridyl ligands [3]. In comparison to the corresponding bpy complexes, the azopyridyl ligands caused a shift in the ligand centered reduction to more positive potentials by 0.8–1.2 V [3]. To explore these results furthermore, more complex systems containing other redox active polypyridyl ligands, needed to be constructed. In line with those results, the desired complex should (i) introduce a redox active substituent to the central pyridyl unit of a tpy ligand and (ii) introduce new monodentate ligands to the sixth position of the complexes to control the electron density of the metal center. Combining both of these desired features will make it possible to change the redox potentials and charge transfer energies of the complexes as desired. The aim is to produce a complex which demonstrates a new functionality derived from electronic communication between the metal center and ligand redox active site.

A candidate for substitution on the terpyridine unit is the redox active *p*-dimethoxyphenyl unit positioned at the 4′-position, which has been previously prepared by Colbran and co-workers [4]. Changes have also be made in the sixth ligand so that it exhibits one of three different electronic properties: π-electron donor (Cl), π-electron acceptor (CO) and an intermediate (CH_3CN). In this paper, the synthesis, structures and redox properties of $[Ru(tpyOMe)(bpy)L]^{n+}$ (tpyOMe = 4′-(2,5-dimethoxyphenyl)-2,2′:6′,2″-terpyridine, L = Cl ($[\mathbf{1}]^+$), CH_3CN ($[\mathbf{2}]^{2+}$), CO ($[\mathbf{3}]^{2+}$)) complexes is described. Furthermore, the kinetic studies regarding ligand replacement reactions are also reported to elucidate the Cl dissociation rate and mechanistic assignments under various conditions.

2. Experimental

2.1. Physical and kinetic measurements

Elemental analyses were carried out at the Research Center for Molecular-Scale Nanoscience, Institute for Molecular Science. IR spectra were obtained as KBr pellets with a JASCO FT-IR 4100 spectrometer. Mass spectra were obtained with a Bruker Daltonics microTOF mass spectrometer equipped with electrospray ionization (ESI) interface. Electronic absorption spectra were obtained in 1 cm quartz cuvettes on a JASCO V-570 UV/VIS/NIR spectrophotometer. NMR spectra were recorded on a JEOL JMN-AL300 spectrometer operating at the ^1H and ^{13}C frequencies of 300 and 75.5 MHz, respectively. Chemical shifts were reported in parts per million downfield from tetramethylsilane (TMS) as referenced

---

* Corresponding author. Tel./fax: +81 24 548 8199.
E-mail address: daio@sss.fukushima-u.ac.jp (D. Oyama).

0277-5387/$ - see front matter © 2009 Elsevier Ltd. All rights reserved.
doi:10.1016/j.poly.2009.12.024

from the residual solvent peaks. Electrochemical measurements were conducted on an ALS/Chi model 620A electrochemical analyzer. Measurements on complexes were made in CH_3CN containing tetra-*n*-butylammonium perchlorate (0.1 M) as a supporting electrolyte, in a one-compartment cell consisting of a platinum working electrode, a platinum wire counter electrode, and an Ag/$AgNO_3$ (0.01 M in CH_3CN) reference electrode. Cyclic voltammograms were obtained at a sweep rate of 0.1 V/s. All potentials are reported in volts versus ferrocenium/ferrocene couple (Fc^+/Fc) at 25 °C under N_2. The $E_{1/2}$ values were calculated as an average of the oxidative and reductive peak potentials, $(E_{pa} + E_{pc})/2$. Kinetic measurements were carried out at 40, 50 or 60 ± 1 °C in a constant temperature bath. Stock solutions of $[Ru(tpyOMe)(bpy)Cl]^+$ ($[\mathbf{1}]^+$) were prepared in RCN (R = CH_3, C_2H_5, C_3H_7 or C_6H_5)–CH_3OH (or H_2O) mixtures under N_2. The complex concentration was 1.0×10^{-4} M. A portion of the solution was transferred by syringe to the UV–Vis spectral cuvette and the spectrum of the sample was recorded at appropriate intervals. Rate data for the substitution were obtained by monitoring the absorbance increase at ca. 460 nm and absorbance decrease at 508 nm. A_f was measured when the intensity changes stopped. Values of pseudo-first order rate constants (k_{obs}) were obtained from the slopes of the plots of $\ln(A_f - A_t)$ or $-\ln(A_f - A_t)$ against time [5].

2.2. Preparation of compounds

All solvents were purchased as anhydrous solvents for organic synthesis and used without further purification. CH_3CN for electrochemical experiments was further distilled over CaH_2 under N_2 just prior to use. 4′-(2,5-dimethoxyphenyl)-2,2′:6′,2′′-terpyridine (tpyOMe) and $[Ru(DMSO)_4Cl_2]$ (DMSO = dimethyl sulfoxide) were prepared according to known procedures or a modification of such a method [4,6].

2.2.1. [Ru(tpyOMe)(DMSO)Cl₂]

The complex was prepared by modification of a previously reported method [7]. $[Ru(DMSO)_4Cl_2]$ (100 mg, 0.21 mmol) was dissolved in methanol (5 mL) under Ar, and the mixture was refluxed for 10 min. TpyOMe (77 mg, 0.21 mmol) was slowly added to the refluxing solution. The solution was refluxed for a further 10 h. The mixture was allowed to cool, and the brown precipitate was collected by filtration, washed with water (to remove $[Ru(tpyOMe)_2]^{2+}$) and methanol, and then dried *in vacuo*. Yield 95 mg (71%).

2.2.2. [Ru(tpyOMe)(bpy)Cl]X ([**1**]Cl and [**1**]PF₆)

$[Ru(tpyOMe)(DMSO)Cl_2]$ (60 mg, 0.10 mmol) and bpy (16 mg, 0.10 mmol) were added to methanol (50 mL) and the suspension was refluxed for 1 h. The volume was reduced to 10 mL using a rotary evaporator, and purple crystals were precipitated by addition of diethyl ether. The precipitate was collected by filtration, washed with diethyl ether and dried *in vacuo*. The crude product was finally recrystallized from acetonitrile and diethyl ether, yielding [Ru(tpyOMe)(bpy)Cl]Cl as a purple powder. Yield 56 mg (80%). The corresponding PF_6 salt was prepared by addition of a saturated aqueous solution of KPF_6 to a methanolic solution of [Ru(tpyOMe)(bpy)Cl]Cl. Yield 58 mg (72%). *Anal.* Calc. for $C_{33}H_{27}N_5O_2F_6PClRu \cdot H_2O$: C, 48.04; H, 3.54; N, 8.49. Found: C, 47.72; H, 3.50; N, 8.50%. ESI-MS (CH_3CN): *m*/*z* = 662 ($[M]^+$). ^1H NMR (CD_3CN): δ 10.22 (d, 1H), 8.70 (s, 2H), 8.62 (d, 1H), 8.44 (d, 2H), 8.33 (d, 1H), 8.25 (t, 1H), 7.94–7.84 (m, 3H), 7.70–7.65 (m, 3H), 7.37–7.09 (m, 6H), 6.97 (t, 1H), 3.94 (s, 3H) and 3.89 (s, 3H) ppm. $^{13}C\{^1H\}$ NMR (CD_3CN): δ 159.78–159.69 (multiple signals), 158.28, 157.11, 155.01, 153.39–152.85 (multiple signals), 151.95, 144.78, 138.89, 137.82, 137.32, 136.36, 128.27–127.73 (multiple signals), 126.93, 124.43–123.90 (multiple signals), 116.58, 114.08, 56.93 and 56.50 ppm.

2.2.3. [Ru(tpyOMe)(bpy)(CH₃CN)](PF₆)₂ ([**2**](PF₆)₂)

[**1**]Cl (60 mg, 0.09 mmol) was dissolved in water (10 mL)-methanol (10 mL)-acetonitrile (4 mL) mixture. This was refluxed for 2 h, before being reduced to 6 mL using a rotary evaporator. Red crystals precipitated when a saturated aqueous solution of KPF_6 was added to the concentrated mixture. The precipitate was collected by filtration, washed with diethyl ether and dried *in vacuo*. The crude product was recrystallization from methanol/diethyl ether to give large crystals of $[Ru(tpyOMe)(bpy)(CH_3CN)](PF_6)_2$. Yield 53 mg (64%). *Anal.* Calc. for $C_{35}H_{30}N_6O_2F_{12}P_2Ru \cdot 0.5CH_3CN$: C, 44.20; H, 3.25; N, 9.31. Found: C, 43.77; H, 3.36; N, 9.27%. ESI-MS (CH_3CN): *m*/*z* = 328 ($[M{-}CH_3CN{+}N_2]^{2+}$). ^1H NMR (CD_3CN): δ 9.61 (d, 1H), 8.78 (s, 2H), 8.62 (d, 1H), 8.47 (d, 2H), 8.35 (t, 2H), 8.02–7.94 (m, 3H), 7.81 (t, 1H), 7.69 (d, 2H), 7.37–7.08 (m, 7H), 3.95 (s, 3H) and 3.90 (s, 3H) ppm. $^{13}C\{^1H\}$ NMR (CD_3CN): δ 159.48–158.60 (multiple signals), 157.90, 156.88, 155.32, 155.05, 154.10, 153.38, 151.95, 148.05, 139.87, 139.39, 138.54, 138.29, 128.83, 128.67, 128.44, 127.60, 127.20, 126.12, 125.20–124.85 (multiple signals), 124.46, 124.21, 117.71, 117.13, 114.25, 56.98 and 56.55 ppm.

2.2.4. [Ru(tpyOMe)(bpy)(CO)](PF₆)₂ ([**3**](PF₆)₂)

A suspension of $[\mathbf{2}](PF_6)_2$ (50 mg, 0.05 mmol) in 2-methoxyethanol (30 mL) was heated to 100 °C under an atmosphere of CO (25 atm) for 1 week. The reaction mixture was reduced to 5 mL using a rotary evaporator. Addition of diethyl ether to the solution resulted in the formation of a light brown precipitate of $[Ru(tpyOMe)(bpy)(CO)](PF_6)_2$. The product was collected by filtration and washed with diethyl ether and dried *in vacuo*. The crude product was purified by diffusion of diethyl ether into an acetone solution of the compound. Yield 33 mg (67%). *Anal.* Calc. for $C_{34}H_{27}N_5O_3F_{12}P_2Ru$: C, 43.23; H, 2.88; N, 7.42. Found: C, 43.15; H, 3.03; N, 7.48%. ESI-MS (CH_3CN): *m*/*z* = 328 ($[M]^{2+}$). IR (KBr): 1982 and 1995 (sh) cm^{-1} ($\nu C{\equiv}O$). ^1H NMR (CD_3CN): δ 9.58 (d, 1H), 8.81 (s, 2H), 8.64 (d, 1H), 8.52–8.48 (m, 3H), 8.39 (t, 1H), 8.16–8.06 (m, 3H), 7.95 (t, 1H), 7.73 (d, 2H), 7.45–7.17 (m, 7H), 3.94 (s, 3H) and 3.90 (s, 3H) ppm. $^{13}C\{^1H\}$ NMR (CD_3CN): δ 194.65 (CO), 158.38, 156.46, 156.17, 155.82, 155.04, 154.75, 151.98–151.93 (multiple signals), 148.63, 141.63, 141.32, 140.55, 129.52–129.42 (multiple signals), 128.87, 126.47–126.09 (multiple signals), 125.20, 117.89, 117.62, 114.36, 57.03 and 56.56 ppm.

2.3. X-ray crystallography

The single crystals of $[\mathbf{2}]^{2+}$ and $[\mathbf{3}]^{2+}$ were obtained by a week-long diffusion of diethyl ether into an acetonitrile solution ($[\mathbf{2}]^{2+}$) or an acetone solution ($[\mathbf{3}]^{2+}$) of the complexes. An orange crystal of $[\mathbf{2}](PF_6)_2 \cdot CH_3CN$ with the dimensions 0.3 × 0.2 × 0.1 mm was mounted on a glass fiber. The crystals of $[\mathbf{3}]^{2+}$ exhibited two distinct colors and habits. A yellow needle-like crystal with the dimensions 0.4 × 0.1 × 0.1 mm was revealed to be $[\mathbf{3}](PF_6)_2 \cdot (CH_3)_2CO$. A red block-like crystal with the dimensions 0.6 × 0.2 × 0.2 mm was revealed to be $[\mathbf{3}](PF_6)_2$. All data were collected on a Rigaku RAXIS-RAPID diffractometer with graphite monochromated Mo Kα radiation ($\lambda = 0.71075$ Å). Data were collected to a maximum 2θ value of 55.0°. All calculations were carried out using the CRYSTALSTRUCTURE crystallographic software package [8]. The structures were solved either by direct methods ($[\mathbf{2}](PF_6)_2 \cdot CH_3CN$ and $[\mathbf{3}](PF_6)_2$) [9] or by the Patterson method ($[\mathbf{3}](PF_6)_2 \cdot (CH_3)_2CO$) [10], and both were expanded using Fourier techniques. Multi-scan absorption corrections were applied [11]. The non-hydrogen atoms (other than F atoms of counter anions and C and N atoms of the solvent molecule (CH_3CN) in the case of $[\mathbf{2}](PF_6)_2 \cdot CH_3CN$) were refined anisotropically, and hydrogen atoms included as riding atoms. One of the anions was disordered over two positions around an F–P–F bond axis in $[\mathbf{2}](PF_6)_2 \cdot CH_3CN$.

Table 1
Crystallographic data for [**2**]$(PF_6)_2\cdot CH_3CN$, [**3**]$(PF_6)_2\cdot (CH_3)_2CO$ and [**3**]$(PF_6)_2$.

	[**2**]$(PF_6)_2\cdot CH_3CN$	[**3**]$(PF_6)_2\cdot (CH_3)_2CO$	[**3**]$(PF_6)_2$
Chemical formula	$C_{37}H_{33}N_7O_2F_{12}P_2Ru$	$C_{37}H_{33}N_5O_4F_{12}P_2Ru$	$C_{34}H_{27}N_5O_3F_{12}P_2Ru$
Formula weight	998.71	1002.70	944.62
Temperature (K)	173(1)	173(1)	173(1)
Crystal system	triclinic	triclinic	monoclinic
Space group	$P\bar{1}$ (no. 2)	$P\bar{1}$ (no. 2)	$P2_1/n$ (no. 14)
Unit cell parameters			
a (Å)	8.8827(8)	9.1389(5)	8.84218(16)
b (Å)	12.4297(12)	14.9718(7)	25.0491(5)
c (Å)	19.3308(18)	15.3166(7)	16.3475(3)
α (°)	71.420(3)	103.6671(17)	
β (°)	85.567(2)	95.1080(16)	90.3548(7)
γ (°)	87.007(3)	104.5294(14)	
V (Å^3)	2016.1(3)	1946.58(17)	3620.72(12)
Z	2	2	4
μ (Mo Kα) (cm^{-1})	5.681	5.910	6.276
Number of measured reflections	18831	19031	34966
Number of observed reflections	5355 ($I > 1.2\sigma(I)$)	5972 ($I > 1.0\sigma(I)$)	6883 ($I > 2.0\sigma(I)$)
Refinement method	Full-matrix least-squares on F^2		
Parameters	532	583	541
R_1[a]	0.0872	0.0549	0.0348
wR_2[b]	0.2308 ($I > 1.2\sigma(I)$)	0.1192 (($I > 1.0\sigma(I)$))	0.1087 ($I > 2.0\sigma(I)$)
S	1.002	1.015	1.008

[a] R_1 ($I > 2\sigma(I)$) = $\Sigma||F_o| - |F_c||/\Sigma|F_o|$.
[b] $wR_2 = \{\Sigma_w(F_o^2 - F_c^2)^2/\Sigma_w(F_o^2)^2\}^{1/2}$.

Table 2
UV–Vis spectral and electrochemical data for the present complexes.

	Complexes		
	[**1**]$^+$	[**2**]$^{2+}$	[**3**]$^{2+}$
λ_{max}/nm[a] (ε/M^{-1} cm^{-1})	508 (11600)	464 (13500)	387 (8700)
	362 (sh)	308 (33800)	315 (25900)
	318 (28800)	283 (44500)	287 (43000)
	292 (37100)		267 (32700)
	283 (42200)		
E/V[b]			
Ru$^{III/II}$[c]	0.38	0.88	
tpyOMe$^{+/0}$[d]	1.04	1.02	1.04
(bpy or tpy)$^{0/-}$ (1)[e]	−1.84	−1.70	−1.45
(bpy or tpy)$^{0/-}$ (2)[e]	−1.98	−2.01	−1.76

[a] In CH_3CN.
[b] In CH_3CN, versus Fc^+/Fc.
[c] $E_{1/2}$ values.
[d] E_{pa} values.
[e] E_{pc} values.

Crystallographic parameters of [**2**]$(PF_6)_2\cdot CH_3CN$, [**3**]$(PF_6)_2\cdot (CH_3)_2CO$ and [**3**]$(PF_6)_2$ are summarized in Table 1 and selected bond lengths and angles are listed in Table 3.

3. Results and discussion

3.1. Synthesis and characterization of [Ru(tpyOMe)(bpy)L]$^{n+}$

Complexes [**1**]$^+$, [**2**]$^{2+}$ and [**3**]$^{2+}$ containing the tpyOMe ligand were prepared as shown in Scheme 1. [Ru(tpyOMe)(DMSO)Cl_2] was adopted as the precursor for the preparation of ruthenium(II) complexes having both tridentate tpyOMe and bidentate bpy. The reaction of [Ru(tpyOMe)(DMSO)Cl_2] with bpy in hot methanol gave [**1**]Cl, and the subsequent exchange of counter anion from Cl^- to PF_6^- gave [**1**]PF_6 in a good yield. [**1**]$^+$ can be also synthesized by the reaction of bpy with [Ru(tpyOMe)Cl_3] which is prepared from $RuCl_3$ and tpyOMe. However, the [Ru(tpyOMe)Cl_3] route gave a much lower yield. [**1**]$^+$ reacts with CH_3CN in H_2O–CH_3OH–CH_3CN mixtures at reflux to give [**2**]$^{2+}$, but does not proceed in CH_3CN only. The details of this replacement reaction are described in Section 3.3. Although [**2**]$^{2+}$ has a labile CH_3CN molecule as a ligand, it required severe conditions (high pressure of CO, high temperature and longer reaction time) to form [**3**]$^{2+}$ using a ligand replacement reaction in CO gas. The IR spectrum of [**3**]$^{2+}$ displays a strong ν(C≡O) band at 1982 cm^{-1}. This value is 22 cm^{-1} lower than that of the corresponding tpy complex ([Ru(tpy)(bpy)(CO)]$^{2+}$) [12] due to the presence of the electron donating dimethoxyphenyl moiety. In addition to this band, a small shoulder band at higher wavenumber side was observed. ESI-MS and ^{1}H NMR spectra show only a single species in solution; however two different solid states would exist from the IR measurement.

The electronic spectra of [**1**]$^+$, [**2**]$^{2+}$ and [**3**]$^{2+}$ in acetonitrile are shown in Fig. 1, and the data are summarized in Table 2. The intense bands in the visible region result from the metal-to-ligand charge transfer (MLCT) transitions, and terpyridyl- and bipyridyl-centered π–π^* transitions are observed in the region between 200 and 350 nm [13]. Although no significant substituent effect was observed between [Ru(tpyOMe)$_2$]$^{2+}$ and [Ru(tpy)(tpyOMe)]$^{2+}$ in the energy of the MLCT transition [4b], the present complex system exhibited very different energies: the absorption at λ_{max} = 508 nm of [**1**]$^+$ is red-shifted by 44 nm relative to [**2**]$^{2+}$, and the MLCT band of [**3**]$^{2+}$ (λ_{max} = 387 nm) is blue-shifted by 77 nm relative to [**2**]$^{2+}$. The change in the MLCT transitions to higher energies (L = CO > CH_3CN > Cl) obeys the spectrochemical series. Thus, changing the ligand L has changed the energies of the MLCT bands, suggesting that substitution of these ligands has an effect on the metal center and moves the dπ orbital energies of the ruthenium(II). Other studies on ruthenium complexes with polypyridyl ligands have attributed this change to a stabilization of the metal dπ orbitals by the π-acceptor ligands which decreases the d–π^* orbital separation [14]. CH_3CN solutions of the complexes showed no detectable room-temperature luminescence when excited at their MLCT maxima.

Single crystal X-ray studies of [**1**]$^+$, [**2**]$^{2+}$ and two polymorphs of [**3**]$^{2+}$ have been conducted. The molecular structure of [**1**]$PF_6\cdot CH_3CN$ has been reported elsewhere [15]. Molecular projections of the structures are shown in Fig. 2 ([**2**]$^{2+}$) and Fig. 3 ([**3**]$^{2+}$), and selected parameters can be found in Table 3. For all the cations, the ligand environment about the ruthenium atom is identical to other [Ru(tpy)(bpy)X]$^{n+}$ complexes (Table 3) [15,16]. The pendant

Table 3
Selected bond lengths (Å) and angles (°) for [**2**](PF_6)$_2$·CH_3CN, [**3**](PF_6)$_2$·$(CH_3)_2CO$ and [**3**](PF_6)$_2$.

	[**2**](PF_6)$_2$·CH_3CN		[**3**](PF_6)$_2$·$(CH_3)_2CO$		[**3**](PF_6)$_2$	
Bond lengths	Ru1–N1	2.079(7)	Ru1–N1	2.078(3)	Ru1–N1	2.1025(19)
	Ru1–N2	1.950(9)	Ru1–N2	1.986(3)	Ru1–N2	1.9848(18)
	Ru1–N3	2.067(6)	Ru1–N3	2.090(3)	Ru1–N3	2.0841(18)
	Ru1–N4	2.089(9)	Ru1–N4	2.068(3)	Ru1–N4	2.083(2)
	Ru1–N5	2.024(8)	Ru1–N5	2.102(4)	Ru1–N5	2.1128(19)
	Ru1–N6	2.045(8)	Ru1–C34	1.856(5)	Ru1–C34	1.882(2)
	O1–C21	1.361(12)	C34–O3	1.152(10)	C34–O3	1.132(3)
	O1–C23	1.434(13)	C17–O1	1.374(6)	C18–O1	1.377(3)
	O2–C18	1.371(13)	O1–C22	1.436(6)	O1–C22	1.414(4)
	O2–C22	1.410(18)	C20–O2	1.381(6)	C21–O2	1.373(3)
			O2–C23	1.425(5)	O2–C23	1.433(3)
Bond angles	C21–O1–C23	116.8(9)	Ru1–C34–O3	177.0(3)	Ru1–C34–O3	177.4(2)
	C18–O2–C22	117.7(9)	C17–O1–C22	117.5(3)	C18–O1–C22	117.6(2)
			C20–O2–C23	117.2(4)	C21–O2–C23	116.5(2)
Dihedral angle	43.0(3)		55.92(17)		45.01(9)	

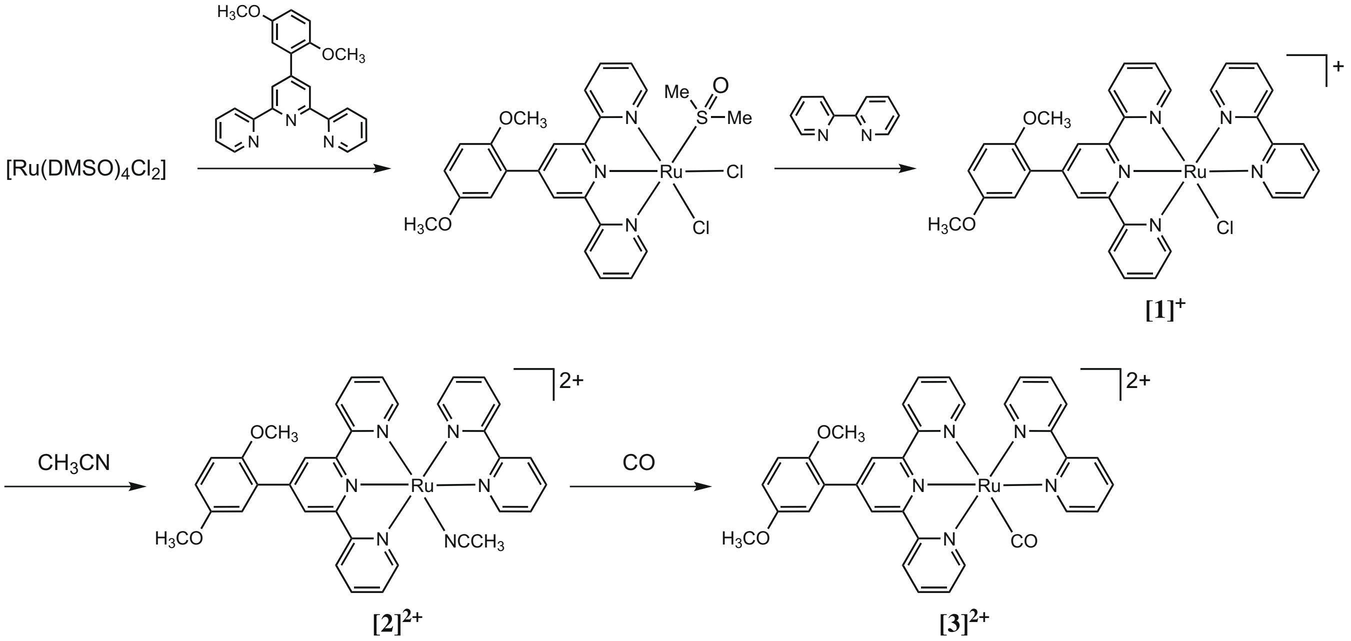

Scheme 1.

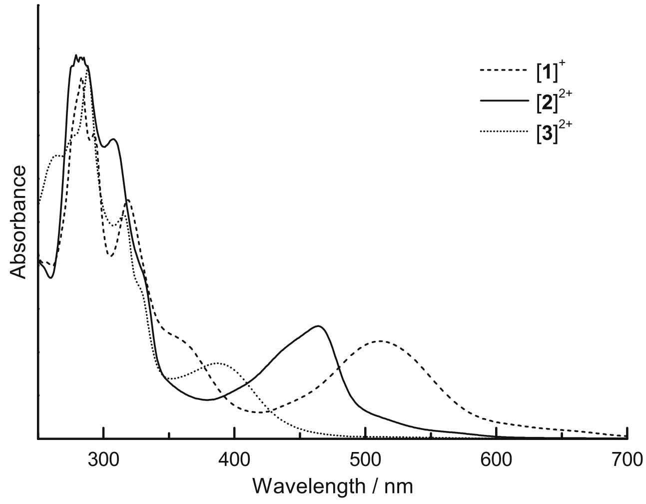

Fig. 1. Electronic spectra of [**1**]$^+$, [**2**]$^{2+}$ and [**3**]$^{2+}$ ($c = 1.0 \times 10^{-4}$ M in CH_3CN).

dimethoxyphenyl substituents are not coplanar with the terpyridyl moiety; the dihedral angles between the central pyridyl and the dimethoxyphenyl ring are 43.0–55.9°. This is comparable to that found for the metal-free ligand (50.2°) [4b]. Fig. 2 depicts the molecular structure of [**2**]$^{2+}$. There are no significant differences in the Ru–$NCCH_3$ moiety compared with the analogous complex ([Ru(tpy)(bpy)(CH_3CN)]$^{2+}$) [16a].

Crystals, with two different habits (yellow needles and red blocks) were separated from the recrystallization of [**3**]$^{2+}$. The different crystal habits had different space groups with the yellow crystals solving in $P\bar{1}$ as [**3**](PF_6)$_2$·$(CH_3)_2CO$, and the red crystals solving in $P2_1/n$ as [**3**](PF_6)$_2$. A comparison of the ruthenium geometries in the two structures is shown in Table 3 and Fig. 3a and b. The geometries around the ruthenium atom are similar to each other and are consistent with those observed in closely related complex ([Ru(tpy)(bpy)(CO)](PF_6)$_2$: Ru–C, 1.844(4) Å; C–O, 1.160(4) Å; Ru–C–O, 175.2(3)°) [12]. However, the O–CH_3 orientation of two methoxy groups are different: two O–CH_3 groups point in the same orientation in [**3**](PF_6)$_2$·$(CH_3)_2CO$ (Fig. 3a), while in [**3**](PF_6)$_2$ they point in opposite directions (Fig. 3b). The former structure is identical to [**1**]$^+$ and [**2**]$^{2+}$. On the other hand, the latter

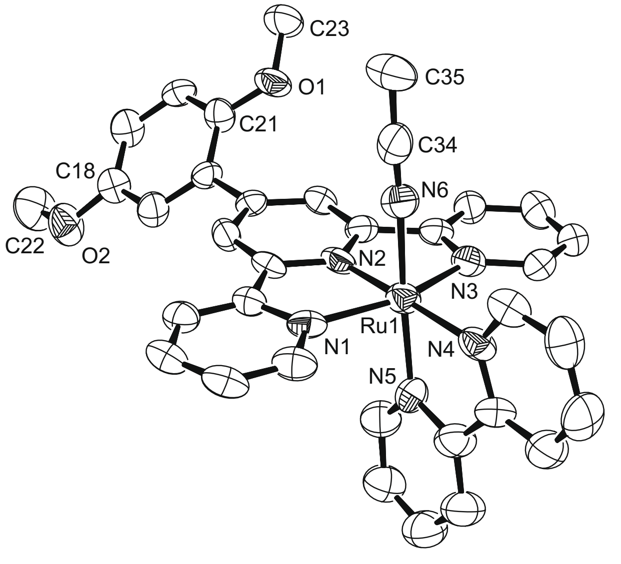

Fig. 2. ORTEP drawing of $[Ru(tpyOMe)(bpy)(CH_3CN)]^{2+}$ ($[\mathbf{2}]^{2+}$) with the atom numbering scheme. Hydrogen atoms have been omitted for clarity. The thermal ellipsoids are shown at the 50% probability level.

form is consistent with that observed in the metal-free tpyOMe and its copper(II) complex [4b]. These differences are most likely due to different packing or intermolecular effects on the orientation of methoxy groups of the tpyOMe ligand [17].

3.2. Redox properties

The electrochemical potentials of $[\mathbf{1}]^+$, $[\mathbf{2}]^{2+}$ and $[\mathbf{3}]^{2+}$ were characterized by cyclic voltammetry experiments in CH_3CN solution, and the results are summarized in Table 2. Fig. 4 shows cyclic voltammograms for the present complexes. All three complexes show a quasi-reversible one-electron oxidation attributed to the dimethoxyphenyl group at ca. +1.0 V. This value remains constant even when a wide variety of ligands are introduced into the complexes (c.f. tpyOMe → $tpyOMe^+$ is oxidized at +1.05 V in $[Ru(tpyOMe)_2]^{2+}$ and at +1.06 V in $[Ru(tpy)(tpyOMe)]^{2+}$ [4b]). On the other hand, the potentials for the $Ru^{III/II}$ couple varies with the monodentate ligand L: the $Ru^{III/II}$ couple in $[\mathbf{2}]^{2+}$ is 500 mV higher than that of $[\mathbf{1}]^+$, and the $Ru^{III/II}$ couple of $[\mathbf{3}]^{2+}$ was not observed with the solvent window. The change in the potential is reasonably well correlated with the electron-accepting ability of the ligand L. These results suggest no electronic interaction between the L ligand and the dimethoxyphenyl moiety, but the substituent L does effect the metal-centered potentials of the complex. In addition to two oxidation processes, two successive one-electron reduction processes were observed at negative potentials. These are attributed to reduction of the terpyridyl and bipyridyl centers.

3.3. Ligand replacement reaction

In general, the chloride ligands in ruthenium(II) complexes are inert and Ag^+ ions or irradiation of light is required to effect substitution. As described in Section 3.1, no replacement reaction of $[\mathbf{1}]^+$ was observed when CH_3CN solutions were heated. On the other hand, purple solutions of $[\mathbf{1}]^+$ became red in the presence of CH_3OH or H_2O (Eq. (1)).

$$[Ru(tpyOMe)(bpy)Cl]^+ + CH_3CN \xrightarrow{k_{obs}} [Ru(tpyOMe)(bpy)(CH_3CN)]^{2+} + Cl^- \qquad (1)$$

The well-separated absorption maxima for $[\mathbf{1}]^+$ and $[\mathbf{2}]^{2+}$ allowed their interchange to be followed spectrophotometrically. Therefore, the kinetics of the reaction have been monitored by UV–Vis spectroscopy to determine the rate constants and to obtain mechanistic evidence. Fig. 5 illustrates a set of curves which were obtained starting with $[\mathbf{1}]^+$ in $CH_3CN–H_2O$ at 60 °C. The original bands at 360 and 508 nm decreased, and new bands for $[\mathbf{2}]^{2+}$ increased at 308 and 464 nm with clear isosbestic points. Plots of the absorption data (ln(Δabsorbance)) versus time are linear, indicating that this reaction can be described with a first-order rate constant k_{obs}. In principle, the rate constants k_{obs} are pseudo-first order because the

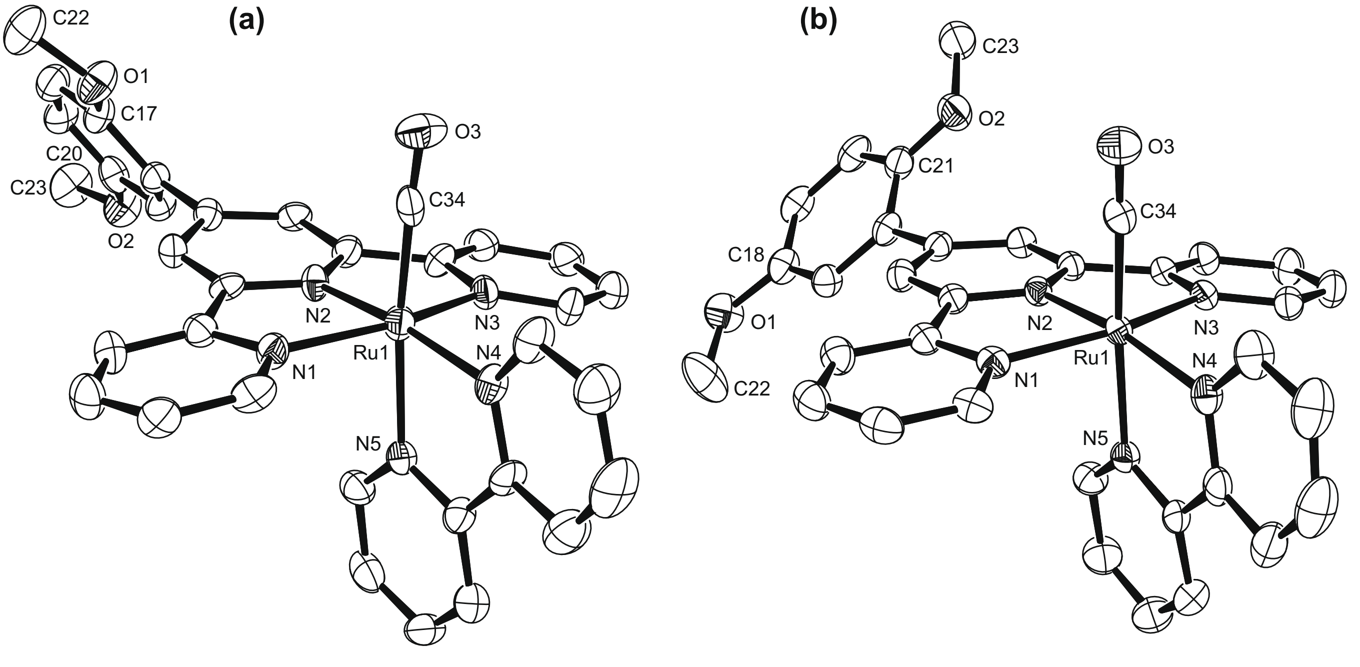

Fig. 3. ORTEP drawings of $[Ru(tpyOMe)(bpy)(CO)]^{2+}$ ($[\mathbf{3}]^{2+}$) with the atom numbering scheme. (a) $[\mathbf{3}](PF_6)_2 \cdot (CH_3)_2CO$, (b) $[\mathbf{3}](PF_6)_2$. Hydrogen atoms have been omitted for clarity. The thermal ellipsoids are shown at the 50% probability level.

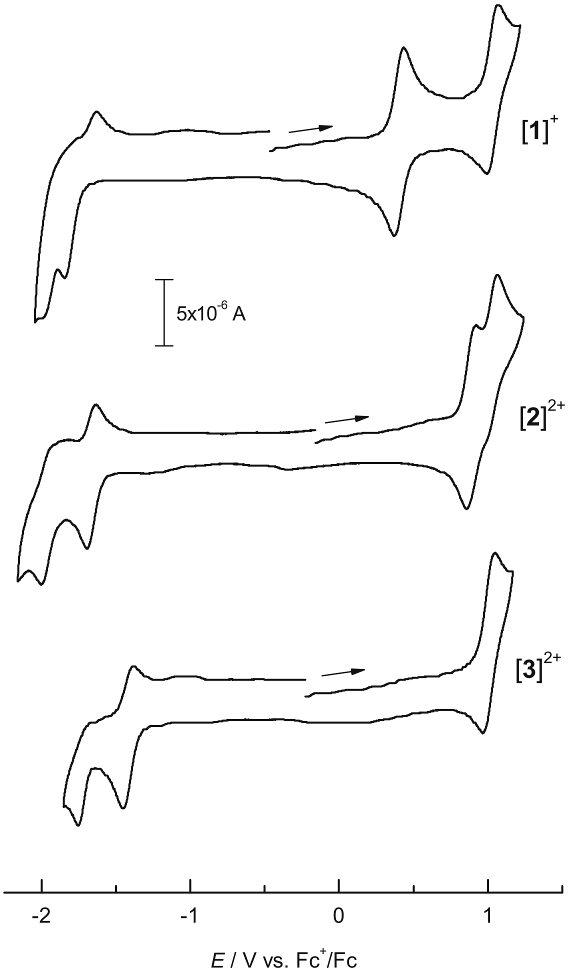

Fig. 4. Cyclic voltammograms of [**1**]+, [**2**]2+ and [**3**]2+ (scan rate = 0.1 V s^{-1}).

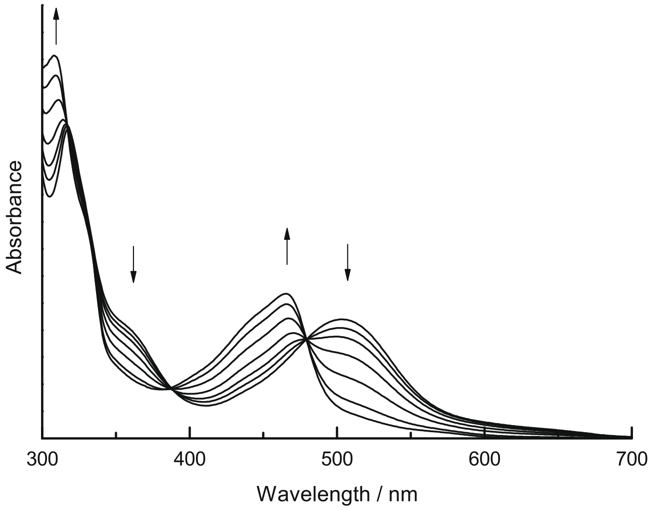

Fig. 5. Time dependence of the electronic spectra of [**1**]+ in $CH_3CN–H_2O$ (1:1 v/v) (1.0×10^{-4} M) at 60 °C recorded at t = 0, 15, 30, 60, 120, 240 and 480 min.

entering ligand concentrations were always much larger than that of [**1**]+. The rate law for the Eq. (1), therefore, is given by

$$\text{Rate} = k_{\text{obs}}[\text{Ru(tpyOMe)(bpy)Cl}] \tag{2}$$

Table 4
Summary of the Cl-replacement reaction rate constants for [**1**]+.

T (°C)	Solvent	RCN	Solv:RCN (v/v)	10^5 k(s^{-1})
60	MeOH	CH_3CN	1:1	2.7
50	MeOH	CH_3CN	1:1	1.5
40	MeOH	CH_3CN	1:1	0.6
60	MeOH	CH_3CN	5:1	4.3
60	MeOH	CH_3CN	10:1	4.5
60	MeOH	C_2H_5CN	1:1	2.7
60	MeOH	C_3H_7CN	1:1	2.7
60	MeOH	C_6H_5CN	1:1	2.7
60	H_2O	CH_3CN	1:1	9.4
50	H_2O	CH_3CN	1:1	7.2
40	H_2O	CH_3CN	1:1	2.9

Under the same conditions, the rate for the replacement reaction of the chloride in the analogous complex ([Ru(tpy)(bpy)Cl]+) was slower than that of [**1**]+. The strong electron donors could stabilize the coordination number-decreasing state, that is, transition states [18]. This result based on the spectator ligand effect, therefore, suggests that increase of electron density of the metal due to the replacement of the tpy ligand to the tpyOMe ligand (more electron donor) caused an acceleration of both dissociation of the Ru–Cl bond and formation of Cl$^-$.

The reaction was also studied using different concentrations or kinds of entering ligands (RCN). The values of k_{obs} for all of the reactions were found to be independent of concentration and the nature of the entering ligands (Table 4). As a result, this system is consistent with a dissociative (I_{d}) mechanism rather than an associative one. This replacement reaction proceeded in the presence of H_2O or CH_3OH. One explanation is that hydrogen bonds form between the chloride ligand and a hydrogen from the solvent reducing the binding energy of the Ru–Cl bond, leading to dissociation of the ligand [19]. Addition of H_2O to the solution of [**1**]+ accelerated of the replacement reaction more than CH_3OH (Table 4). This is consistent with the strength of the hydrogen bonding. This reaction, therefore, has been classified as a solvent-assisted dissociation (SAD) [20].

Supplementary data

CCDC 749665, 749666 and 749667 contains the supplementary crystallographic data for [**2**]$(PF_6)_2 \cdot CH_3CN$, [**3**]$(PF_6)_2 \cdot (CH_3)_2CO$ and [**3**]$(PF_6)_2$. These data can be obtained free of charge via http://www.ccdc.cam.ac.uk/conts/retrieving.html, or from the Cambridge Crystallographic Data Centre, 12 Union Road, Cambridge CB2 1EZ, UK; fax: (+44) 1223-336-033; or e-mail: deposit@ccdc.cam.ac.uk.

Acknowledgments

Professor Koji Tanaka of the Institute for Molecular Science is acknowledged for helpful discussions and insight. The authors thank the Joint Studies Program (2008–2009) of the Institute for Molecular Science for generous financial support of this research.

References

[1] (a) G. Denti, S. Campagna, L. Sabatino, S. Serroni, M. Caino, V. Balzani, Inorg. Chem. 29 (1990) 4750;
(b) B. Whittle, N.S. Everest, C. Howard, M.D. Ward, Inorg. Chem. 34 (1995) 2025;
(c) N. Sutin, C. Creutz, E. Fujita, Comments Inorg. Chem. 19 (1997) 67;
(d) A.D. Shukla, B. Whittle, H.C. Bajaj, A. Das, M.D. Ward, Inorg. Chim. Acta 285 (1999) 89;
(e) S. Rau, D. Walther, J.G. Vos, Dalton Trans. (2007) 915;
(f) Y. Na, M. Wang, J. Pan, P. Zhang, B. Åkermark, L. Sun, Inorg. Chem. 47 (2008) 2805.

[2] (a) M. Navarro, W.F. De Giovani, J.R. Romero, Tetrahedron 47 (1991) 851;
(b) S.A. Trammell, J.C. Wimbish, F. Odobel, L.A. Gallagher, P.M. Narula, T.J. Meyer, J. Am. Chem. Soc. 120 (1998) 13248;
(c) G.M. Kloster, F.C. Anson, Electrochim. Acta 44 (1999) 2271;
(d) E. Sussuchi, A.A. De Lima, W.F. De Giovani, Polyhedron 25 (2006) 1457;
(e) H.W. Tseng, R. Zong, J.T. Muckerman, R. Thummel, Inorg. Chem. 47 (2008) 11763.

[3] (a) D. Oyama, R. Fujita, S. Yui, Inorg. Chem. Commun. 11 (2008) 310;
(b) D. Oyama, A. Asuma, T. Takase, Inorg. Chem. Commun. 11 (2008) 1097;
(c) D. Oyama, A. Asuma, T. Hamada, T. Takase, Inorg. Chim. Acta 362 (2009) 2581.

[4] (a) G.D. Storrier, S.B. Colbran, D.B. Hibbert, Inorg. Chim. Acta 239 (1995) 1;
(b) G.D. Storrier, S.B. Colbran, D.C. Craig, J. Chem. Soc., Dalton Trans. (1998) 1351.

[5] D. Ooyama, M. Saito, Inorg. Chim. Acta 359 (2006) 800.

[6] E. Alessio, G. Mestroni, G. Nardin, W.M. Attia, M. Calligaris, G. Sava, S. Zorzet, Inorg. Chem. 27 (1988) 4099.

[7] T. Norrby, A. Börje, B. Åkermark, L. Hammarstron, J. Alsins, K. Lashgari, R. Norrestam, J. Mårtensson, G. Stenhagen, Inorg. Chem. 36 (1997) 5850.

[8] CRYSTALSTRUCTURE 3.8: Crystal Structure Analysis Package, Rigaku Americas, The Woodlands, USA, and Rigaku Corporation, Tokyo, Japan, 2007.

[9] SIR97: A. Altomare, M.C. Burla, M. Camalli, G.L. Cascarano, C. Giacovazzo, A. Guagliardi, A.G.G. Moliterni, G. Polidori, R. Spagna, J. Appl. Crystallogr. 32 (1999) 115.

[10] PATTY: P.T. Beurskens, G. Admiraal, G. Beurskens, W.P. Bosman, S. Garcia-Granda, R.O. Gould, J.M.M. Smits, C. Smykalla, The DIRDIF Program System, Technical Report of the Crystallography Laboratory, University of Nijmegen, The Netherlands, 1992.

[11] ABSCOR: T. Higashi, Rigaku Corporation, Tokyo, Japan, 1995.

[12] H. Nagao, T. Mizukawa, K. Tanaka, Inorg. Chem. 33 (1994) 3415.

[13] (a) T.J. Meyer, Pure Appl. Chem. 58 (1986) 1193;
(b) A. Juris, V. Balzani, F. Barigelletti, S. Campagna, P. Belser, A. Von Zelewsky, Coord. Chem. Rev. 84 (1988) 85;
(c) J.P. Sauvage, J.P. Collin, J.C. Chambron, S. Guillerez, C. Coudret, V. Balzani, F. Barigelletti, L. De Cola, L. Flamigni, Chem. Rev. 94 (1994) 993;
(d) C.T. Lin, W. Bottcher, M. Chou, C. Creutz, N. Sutin, J. Am. Chem. Soc. 98 (1976) 6536;
(e) J.R. Winkler, T.L. Netzel, C. Creutz, N. Sutin, J. Am. Chem. Soc. 109 (1987) 2381;
(f) M. Beley, J.P. Collin, J.P. Sauvage, H. Sugihara, F. Heisel, A. Miehe, J. Chem. Soc., Dalton Trans. (1991) 3157.

[14] H.F. Suen, S.W. Wilson, M. Pomerantz, J.L. Walsh, Inorg. Chem. 28 (1989) 786.

[15] D. Oyama, M. Kido, A. Orita, T. Takase, Acta Crystallogr., Sect. E 65 (2009) m1117.

[16] (a) S.C. Rasmussen, S.E. Ronco, D.A. Mlsna, M.A. Billadeau, W.T. Pennington, J.W. Kolis, J.D. Petersen, Inorg. Chem. 34 (1995) 821;
(b) A.L. Spek, A. Gerli, J. Reedijk, Acta Crystallogr., Sect. C 50 (1994) 394;
(c) T. Hamaguchi, Y. Inoue, K. Ujimoto, I. Ando, Polyhedron 27 (2008) 2031;
(d) G. Pourrieux, F. Fagalde, N.E. Katz, T. Parella, J. Benet-Buchholz, A. Llobet, Polyhedron 27 (2008) 2990;
(e) I.M. Dixon, E. Lebon, G. Loustau, P. Sutra, L. Vendier, A. Igau, A. Juris, Dalton Trans. (2008) 5627.

[17] G.B. Deacon, J.M. Patrick, B.W. Skelton, N.C. Thomas, A.H. White, Aust. J. Chem. 37 (1984) 929.

[18] P. Atkins, T. Overton, J. Rourke, M. Weller, F. Armstrong, Inorganic Chemistry, fourth ed. (Japanese ed.), Tokyo Kagaku Dojin, Tokyo, 2008, p. 778.

[19] G.L. Miesller, D.A. Tarr, Inorganic Chemistry, Japanese ed., Maruzen, Tokyo, 2003, p. 536.

[20] F. Basolo, R.G. Pearson, Mechanisms of Inorganic Reactions, second ed. (Japanese ed.), Tokyo Kagaku Dojin, Tokyo, 1971, p. 144.